

Joint ML Time and Frequency Synchronization for Distributed MIMO-Relay Beamforming

Souheib Ben Amor*, Sofiène Affes*, Faouzi Bellili[‡], Usa Vilaiornsawai[†], Liqing Zhang[†], and Peiying Zhu[†]

*INRS-EMT, Université du Québec, Montréal, QC, Canada, Emails: {souheib.ben.amor, affes}@emt.inrs.ca

[‡] University of Toronto, Toronto, ON, Canada, Emails: faouzi.bellili@utoronto.ca

[†]Huawei Technologies Canada Co. Ltd., Kanata, ON, Canada, Emails: {usa.vilaiornsawai, liqing.zhang, peiying.zhu}@huawei.com

Abstract—In this paper, we investigate maximum likelihood (ML) time delay (TD) and carrier frequency offset (CFO) synchronization in multi-node decode-and-forward (DF) cooperative relaying systems operating over time-varying channels (TVCs). This new synchronization scheme is embedded into a distributed multiple input multiple output (MIMO)-relay beamforming transceiver structure to avoid the drawbacks of multidimensional ML estimation at the destination and to minimize the overhead cost. The new technique can be jointly implemented with any Doppler spread estimator in an iterative scheme using a time-constant channel (TCC) based synchronization method at the initialization step. The resulting TD and CFO estimates along with the channel estimates are then fed into a distributed MIMO-relay beamforming transceiver of K single-antenna nodes, for pre-compensation at each node of the transmitted signals, to ensure constructive maximum ratio combining (MRC) at the destination. Simulation results show significant synchronization accuracy improvement over previous distributed multi-node synchronization techniques assuming TCCs. The latter translates into noticeable gains in terms of useful link-level throughput, more so at higher Doppler or with more relaying nodes.

Index Terms—Carrier Frequency Offset (CFO), Time Delay (TD), Time-Varying Channel (TVC), Doppler Spread, Distributed MIMO Relay Beamforming, Cooperation, Collaboration, Decode-and-Forward (DF), Multi-Node Synchronization, Maximum Likelihood (ML).

I. INTRODUCTION

Spatial diversity is a well-known concept allowing to combat the channel fading and increase the overall throughput of communication systems. Such attracting advantage can be achieved through multiple solutions. Cooperative networks provide a distributed solution that avoids some of the difficulties related to traditional multiple input multiple output (MIMO) systems [2]. However, some challenges need to be addressed to ensure constructive cooperation between the relays. One major problem in cooperative relaying systems is multi-node synchronization, both in time and frequency. The latter is crucial for the proper implementation of energy-, spectrum-, and area-efficient distributed MIMO-relay beamforming between a given source-destination link having coverage limitations.

Multiple techniques exist in the open literature [3] providing solutions to alleviate the effect of time-varying channel (TVC) distortions in time, frequency, phase, and amplitude.

Work supported by the NSERC/Huawei Canada/TELUS CRD Grant on 5G-WAVES (Wireless Access Virtualization Enabling Schemes), the DG and CREATE PERSWADE <www.create-perswade.ca> Programs of NSERC, and a Discovery Accelerator Supplement Award from NSERC. It was in part disclosed in a journal version in [1].

On one hand, the works in [4,5] investigate time delay (TD) synchronization while neglecting the carrier frequency offset's (CFO) effect. On the other hand, the solutions introduced in [6,7] deal with multiple CFOs while neglecting the TD effect. Other techniques perform joint estimation of all parameters at the destination in closed-loop cooperative networks [8,9]. Although they could work well in practice, they suffer from high computational complexity since they require solving a multi-dimensional problem that increases with the number of relaying nodes.

Alternative solutions can be considered by relying on distributed collaborative beamforming (DCBF) schemes [10]. Many of these techniques focus on the optimal design of the beamformer's weights while assuming perfect synchronization that leave them extremely vulnerable in practice to phase, frequency, and time offsets. Many other techniques focus on the other hand on combating the misalignment effect at the destination caused by such offsets. In [11], the authors proposed a phase compensation solution based on an iterative bit-feedback approach. In [12], a solution for frequency synchronization in wireless sensor networks (WSN) using a round trip synchronization method was proposed. In [13], a distributed synchronization method was proposed for dense wireless networks using a correlation-based joint TD and CFO estimator. Yet, all the above-mentioned techniques rely on the simplifying time-constant channel (TCC) assumption. In contrast, a broad range of applications require that the terminals act as relaying nodes and, at the same time, fifth-generation (5G) communication systems are expected to support reliable communications at very high velocities reaching 500 Km/h (e.g., in high-speed trains) [14]. For such systems, the conventional TCC assumption leads to severe performance losses. Recently, some other works on DCBF [15, 16] had tackled the challenging problem of multi-node synchronization under TVCs using enhanced versions of one-bit feedback technique. However, they have only addressed phase compensation while assuming perfect TD and CFO estimation. In [17], we recently proposed first a distributed solution for time varying channels. However, it assumes perfect estimation of the Doppler at the destination. Besides, it does not address the need for establishing a transmission protocol to properly schedule the different processing and communication tasks between the source, the relays, and the destination.

Motivated by these facts, we develop in this paper a new decentralised maximum likelihood (ML) synchronization

technique along with a distributed MIMO-relay beamforming design that tackles the challenging TVC case over multi-node relaying transmissions. We develop an iterative solution, referred to as ML TVC-DE (Doppler estimate), that accounts for the practical need to estimate at each relay node the Doppler spread and that develops a detailed protocol that properly orchestrates all processing and communications tasks among the source, the relays, and the destination. The proposed ML TVC solution builds upon a very useful approximation of the channel covariance matrix by a two-ray propagation model. Simulation results show noticeable gains in terms of useful link-level throughput, over previous distributed multi-node synchronization techniques assuming TCCs, more so at higher Doppler or with more distributed MIMO-relay beamforming nodes.

The rest of the paper is organized as follows. In Section II, we introduce the system model. In Section III, we derive the new ML solution of the underlying estimation problem. The distributed MIMO-relay design is presented in Section IV. In Section V, we run exhaustive computer simulations to assess the performance of the proposed distributed synchronization and MIMO-relay beamforming solution both at the component and link levels in terms of estimation accuracy and throughput, respectively. Finally, we draw out some concluding remarks in Section VI.

The notations adopted in this paper are as follows. Vectors and matrices are represented in lower- and upper-case bold fonts, respectively. The shorthand notation $x \sim \mathcal{CN}(m, \sigma^2)$ denotes a complex normal (i.e., Gaussian) distribution with mean m and variance σ^2 . Moreover, $\{\cdot\}^T$ and $\{\cdot\}^H$ denote the conjugate and Hermitian (i.e., transpose conjugate) operators and $\det\{\cdot\}$ returns the determinant of any square matrix. The Euclidean norm of any vector is denoted as $\|\cdot\|$ and \mathbf{I}_N denotes the $(N \times N)$ identity matrix. For any vector \mathbf{x} , $\text{diag}\{\mathbf{x}\}$ refers to the diagonal matrix whose elements are those of \mathbf{x} . For any matrix \mathbf{X} , $[\mathbf{X}]_q$ and $[\mathbf{X}]_{l,k}$ denote its q^{th} column and $(l, k)^{\text{th}}$ entry, respectively. The element-wise product between any two vectors \mathbf{x}_1 and \mathbf{x}_2 is denoted as $\mathbf{x}_1 \odot \mathbf{x}_2$. Moreover, $\{\cdot\}^*$, $\angle\{\cdot\}$, and $|\cdot|$ return the conjugate, angle, and modulus of any complex number, respectively. Finally, $\mathbb{E}\{\cdot\}$ stands for the statistical expectation, j is the imaginary unit (i.e., $j^2 = -1$), and the notation \triangleq is used for definitions.

II. SYSTEM MODEL

Consider a cooperative decode-and-forward (DF) communication system with a source, S , a destination, D , and a MIMO relay of K randomly distributed nodes, R_1, R_2, \dots, R_K , as shown in Fig. 1. The K relays are subject to CFOs and TDs due to the presence of different local oscillators. We denote the CFOs of the K relays by $(\bar{\nu}_1, \bar{\nu}_2, \dots, \bar{\nu}_K) \subset [0, \nu_{\max}]^K$ and their respective TDs by $(\bar{\tau}_1, \bar{\tau}_2, \dots, \bar{\tau}_K) \subset [0, \tau_{\max}]^K$. The parameters, ν_{\max} and τ_{\max} , can be set as large as desired within the vicinity of practical CFO and TD values. The true unknown parameters will also carry the superscripts $(\cdot)^{[sr]}$ and $(\cdot)^{[rd]}$ to indicate the communication link to which they belong, i.e., S to R_k and R_k to D , respectively. Most

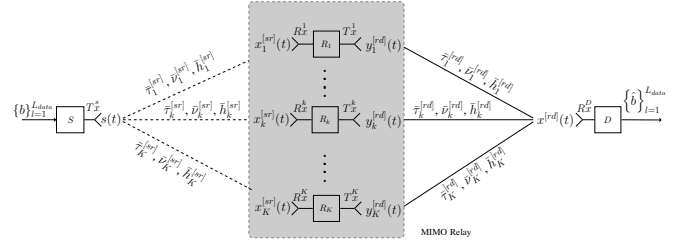


Fig. 1. System model for the distributed MIMO-relay beamforming scheme illustrated during the DT (data transmission) cycles.

importantly, in stark contrast to previous works on multi-node synchronization which have only dealt so far with TCCs, all the nodes and/or the destination are assumed in this work to be mobile, possibly with different velocities. Hence the second-hop's communication link between each relay node R_k and the destination has a TVC characterized by the Doppler σ_{D_k} .

During an initial synchronization period, the final destination starts by broadcasting a common training sequence of L symbols, $\mathbf{a}^{[dr]} \triangleq [a^{[dr]}[1], a^{[dr]}[2], \dots, a^{[dr]}[L]]^T$, to all the relays. Hence, every relay node will be able to estimate its own synchronization parameters locally and independently of all others. During this pilot transmission (PT) period, the destination sends to all relays the following known signal:

$$s^{[dr]}(t) = \sum_{l=0}^{L-1} \mathbf{a}^{[dr]}[l+1]g(t-lT), \quad (1)$$

where $g(t)$ is the shaping pulse and T is the symbol duration. The received signal at the k^{th} relay is given by:

$$x_k^{[dr]}(t) = h_k^{[dr]}(t)s^{[dr]}(t - \bar{\tau}_k^{[dr]})e^{j2\pi\bar{\nu}_k^{[dr]}t} + n_k^{[dr]}(t), \quad (2)$$

where $h_k^{[dr]}(t)$ is a flat-fading Rayleigh channel and $n_k^{[dr]}(t)$ is the additive Gaussian noise component assumed to be temporally white. Using its received signal in (2), each relay will find the estimates, $\hat{\tau}_k^{[dr]}$ and $\hat{\nu}_k^{[dr]}$, for its channel TD and CFO, $\bar{\tau}_k^{[dr]}$ and $\bar{\nu}_k^{[dr]}$, respectively. The signal in (2) is oversampled by a factor $Q = T/T_s$ where T_s is the sampling period. The observation sequence corresponding to the sampling time instants, $\{nT_s\}_{n=0}^{QL-1}$, is given by:

$$x_k^{[dr]}(n) = h_k^{[dr]}(n) \sum_{l=0}^{L-1} \mathbf{a}^{[dr]}[l+1]g(nT_s - lT - \bar{\tau}_k^{[dr]})e^{j2\pi\bar{\nu}_k^{[dr]}\frac{n}{Q}} + n_k^{[dr]}(n), \quad (3)$$

where the additive white Gaussian noise is denoted by $n_k^{[dr]}(n) \sim \mathcal{CN}(0, \sigma_{n_k}^2)$. Notice in (3) that we keep using the same notation, $\bar{\nu}_k^{[dr]}$, as in (2) for the normalized (by T_s) CFO between R_k and D , that is for the sake of simplicity.

In order to rewrite (3) in a matrix/vector form, we denote by $\mathbf{x}_k^{[dr]} \triangleq [x_k^{[dr]}(0), x_k^{[dr]}(1), \dots, x_k^{[dr]}(QL-1)]^T$, $\mathbf{h}_k^{[dr]} \triangleq [h_k^{[dr]}(0), h_k^{[dr]}(1), \dots, h_k^{[dr]}(QL-1)]^T$, and $\mathbf{n}_k^{[dr]} \triangleq [n_k^{[dr]}(0), n_k^{[dr]}(1), \dots, n_k^{[dr]}(QL-1)]^T$ the vectors that contain, respectively, the received samples, the channel coef-

ficients, and the noise components. We also introduce the following matrix parametrized by the generic TD:

$$\mathbf{G}(\tau) \triangleq \begin{pmatrix} g(0-T-\tau) & \dots & g(0-LT-\tau) \\ g(T_s-T-\tau) & \dots & g(T_s-LT-\tau) \\ \vdots & \vdots & \vdots \\ g((QL-1)T_s-T-\tau) & \dots & g((QL-1)T_s-LT-\tau) \end{pmatrix}$$

Starting from (3) and resorting to straightforward algebraic manipulations, we show for $k = 1, 2, \dots, K$ that we have:

$$\mathbf{x}_k^{[dr]} = \mathbf{\Lambda}(\bar{\nu}_k^{[dr]}) \mathbf{\Omega}(\bar{\tau}_k^{[dr]}) \mathbf{h}_k^{[dr]} + \mathbf{n}_k^{[dr]}, \quad (4)$$

where:

$$\mathbf{\Omega}(\tau) \triangleq \text{diag}\{\mathbf{G}(\tau) \mathbf{a}^{[dr]}\}, \quad (5)$$

$$\mathbf{\Lambda}(\nu) \triangleq \text{diag}\left\{ \left[0, e^{j2\pi\nu}, \dots, e^{j2\pi\nu(QL-1)/Q} \right]^T \right\}, \quad (6)$$

For the sake of clarity, we will only focus on the second hop and assume the first hop's estimation and transmission tasks to be ideal. Indeed, the proposed synchronization algorithm can also be applied at each relay node to obtain the matched filtered samples required to decode the data locally during the data transmission (DT) period. As such, we will drop in (4) and in all the equations of the next section the $[dr]$ superscript thereby leading to:

$$\mathbf{x}_k = \mathbf{\Lambda}(\bar{\nu}_k) \mathbf{\Omega}(\bar{\tau}_k) \mathbf{h}_k + \mathbf{n}_k. \quad (7)$$

III. JOINT TD AND CFO ML ESTIMATOR

A. TCC Case

Under the assumption of static channels, all nodes are stationary and as such the Doppler spread is equal to zero. In this case, the system model in (7) reduces to:

$$\mathbf{x}_k = h_k \mathbf{\Lambda}(\bar{\nu}_k) \mathbf{G}(\bar{\tau}_k) \mathbf{a} + \mathbf{n}_k, \quad (8)$$

where h_k is the channel gain of the communication link between D and R_k . It can be shown that the log-likelihood function (LLF) can be expressed as follows:

$$\begin{aligned} \mathcal{L}(\nu_k, \tau_k, h_k, \sigma_{n_k}^2) \\ = -\frac{1}{\sigma_{n_k}^2} \|\mathbf{x}_k - h_k \mathbf{\Psi}(\nu_k, \tau_k) \mathbf{a}\|^2 - QL \ln(\pi \sigma_{n_k}^2), \end{aligned} \quad (9)$$

where

$$\mathbf{\Psi}(\nu_k, \tau_k) = \mathbf{\Lambda}(\nu_k) \mathbf{G}(\tau_k). \quad (10)$$

First, we maximize $\mathcal{L}(\nu, \tau, h, \sigma_{n_k}^2)$ with respect to the noise variance. The partial derivative of (9) with respect to $\sigma_{n_k}^2$ is given by:

$$\frac{\partial}{\partial \sigma_{n_k}^2} \mathcal{L}(\nu_k, \tau_k, h_k, \sigma_{n_k}^2) = \frac{1}{\sigma_{n_k}^4} \|\mathbf{x}_k - h_k \mathbf{\Psi}(\nu_k, \tau_k) \mathbf{a}\|^2 - \frac{QL}{\sigma_{n_k}^2}.$$

Setting this result to zero and solving for $\sigma_{n_k}^2$ yields the ML estimate for the noise variance:

$$\widehat{\sigma}_{n_k, \text{ML}}^2 = \frac{1}{QL} \|\mathbf{x}_k - h_k \mathbf{\Psi}(\nu_k, \tau_k) \mathbf{a}\|^2, \quad (11)$$

which is substituted back in (9) to obtain the following ML estimates for the remaining parameters at each relay node:

$$[\widehat{\nu}_k, \widehat{\tau}_k, \widehat{h}_k] = \underset{\nu, \tau, h}{\text{argmin}} \mathcal{L}(\nu, \tau, h), \quad (12)$$

where:

$$\mathcal{L}(\nu, \tau, h) = \|\mathbf{x}_k - h \mathbf{\Psi}(\nu, \tau) \mathbf{a}\|^2. \quad (13)$$

For any given couple of values for ν and τ , the LLF optimization over h_k reduces to a linear least squares (LS) problem whose solution is given by:

$$\widehat{h}_k = \frac{1}{\|\mathbf{\Psi}(\nu, \tau) \mathbf{a}\|^2} \mathbf{a}^H \mathbf{\Psi}(\nu, \tau)^H \mathbf{x}_k. \quad (14)$$

By substituting \widehat{h}_k for h_k back in (13) and after some algebraic manipulations, we obtain the so-called *compressed* LLF (CLLF) which depends solely on ν and τ :

$$\mathcal{L}_c(\nu, \tau) = \frac{1}{\|\mathbf{\Psi}(\nu, \tau) \mathbf{a}\|^2} \mathbf{x}_k^H \mathbf{\Psi}(\nu, \tau) \mathbf{a} \mathbf{a}^H \mathbf{\Psi}(\nu, \tau)^H \mathbf{x}_k. \quad (15)$$

Hence, the joint ML estimates of ν_k and τ_k become the solution of the following optimization problem:

$$[\widehat{\nu}_k, \widehat{\tau}_k] = \underset{\nu, \tau}{\text{argmax}} \mathcal{L}_c(\nu, \tau). \quad (16)$$

B. TVC Case

We start by deriving the LLF that depends on all the unknown parameters observed separately at each relay, i.e., $\nu_k, \tau_k, h_k, \sigma_{n_k}^2$. Since the noise components are assumed to be temporally white and Gaussian distributed, i.e., $\mathbf{n}_k \sim \mathcal{CN}(\mathbf{0}, \sigma_{n_k}^2 \mathbf{I}_{QL})$, each vector \mathbf{x}_k in (7) is also Gaussian distributed. Hence, it can be shown that the *actual* LLF at each relay R_k , after dropping the constant terms, is given by:

$$\mathcal{L}(\nu_k, \tau_k, h_k, \sigma_{n_k}^2) = -\ln(\det\{\mathbf{R}_{\mathbf{x}_k \mathbf{x}_k}\}) - \mathbf{x}_k^H \mathbf{R}_{\mathbf{x}_k \mathbf{x}_k}^{-1} \mathbf{x}_k, \quad (17)$$

where $\mathbf{R}_{\mathbf{x}_k \mathbf{x}_k} = \mathbb{E}\{\mathbf{x}_k \mathbf{x}_k^H\}$ is the covariance of the zero-mean observation \mathbf{x}_k whose expression follows from (7) as:

$$\mathbf{R}_{\mathbf{x}_k \mathbf{x}_k} = \mathbf{\Lambda}(\nu_k) \mathbf{\Omega}(\tau_k) \mathbf{R}_{\mathbf{h}_k \mathbf{h}_k} \mathbf{\Omega}(\tau_k)^H \mathbf{\Lambda}(\nu_k)^H + \sigma^2 \mathbf{I}_{QL}, \quad (18)$$

where $\mathbf{R}_{\mathbf{h}_k \mathbf{h}_k} = \mathbb{E}\{\mathbf{h}_k \mathbf{h}_k^H\}$. It is obvious that maximizing $\mathcal{L}(\nu_k, \tau_k, h_k, \sigma_{n_k}^2)$ requires the inversion of a large-size ($QL \times QL$) covariance matrix and the computation of its determinant. In the following, we develop a new solution that avoids these costly calculations. Actually, the new solution relies on the two-ray channel approximation¹ of the covariance matrix of the channel, as described in [18,19] (please refer to the Appendix in [18] for more details about the underlying second-order Taylor series approximation), which leads to:

$$\mathbf{R}_{\mathbf{h}_k \mathbf{h}_k} \approx \frac{\sigma_{h_k}^2}{2} \mathbf{W} \mathbf{W}^H, \quad (19)$$

where $\sigma_{h_k}^2$ is channel variance and \mathbf{W} is defined as follows:

$$\mathbf{W} = [\mathbf{w} \quad \mathbf{w}^*]. \quad (20)$$

¹The two-ray channel approximation holds only when $LF_{D_k} T \ll 1$.

The vector \mathbf{w} in (20) is given by:

$$\mathbf{w} = \left[1 \ e^{-j\sigma_{D_k} T_s} \ \dots \ e^{-j(Q_L-1)\sigma_{D_k} T_s} \right]^T.$$

Injecting (19) in (18) leads to the following overall covariance matrix approximation:

$$\mathbf{R}_{\mathbf{x}_k \mathbf{x}_k} = \frac{\sigma_{h_k}^2}{2} \mathbf{\Lambda}(\nu_k) \mathbf{C}(\tau_k) \mathbf{C}^H(\tau_k) \mathbf{\Lambda}(\nu_k)^H + \sigma_{n_k}^2 \mathbf{I}_{Q_L}, \quad (21)$$

in which the matrix $\mathbf{C}(\tau_k)$ is defined as follows:

$$\mathbf{C}(\tau_k) \triangleq [\mathbf{c}_1(\tau_k) \ \mathbf{c}_2(\tau_k)] = \mathbf{\Omega}(\tau_k) \mathbf{W}. \quad (22)$$

To find the inverse of $\mathbf{R}_{\mathbf{x}_k \mathbf{x}_k}$ and its determinant, we start by finding the analytical expressions for the eigenvalues of $\mathbf{C}(\tau_k) \mathbf{C}^H(\tau_k)$ and their corresponding eigenvectors. Clearly, the matrix $\mathbf{C}(\tau_k) \mathbf{C}^H(\tau_k)$ is of rank two and has the same non-zero eigenvalues values as $\mathbf{C}^H(\tau_k) \mathbf{C}(\tau_k)$. Since the latter is a 2×2 matrix, its eigenvalues can be computed analytically. Indeed, it can be shown that:

$$\mathbf{C}^H(\tau_k) \mathbf{C}(\tau_k) = \begin{pmatrix} \alpha(\tau_k) & \varphi(\tau_k) \\ \varphi(\tau_k)^* & \alpha(\tau_k) \end{pmatrix}, \quad (23)$$

where:

$$\alpha(\tau_k) = \sum_{n=0}^{Q_L-1} (\Omega_{n,n}(\tau_k))^2, \quad (24)$$

$$\varphi(\tau_k) = \sum_{n=0}^{Q_L-1} (\Omega_{n,n}(\tau_k))^2 e^{2\sigma_{D_k}(n-1)T_s}. \quad (25)$$

From the roots of the characteristic polynomial of $\mathbf{C}^H(\tau_k) \mathbf{C}(\tau_k)$ in (23), we obtain the two eigenvalues as:

$$\lambda_1 = \alpha(\tau_k) + |\varphi(\tau_k)| \quad \text{and} \quad \lambda_2 = \alpha(\tau_k) - |\varphi(\tau_k)|. \quad (26)$$

Hence, the corresponding unit-norm eigenvectors are given by:

$$\mathbf{v}_1 = \frac{1}{\sqrt{2}} \begin{bmatrix} 1 \\ \frac{\varphi(\tau_k)^*}{|\varphi(\tau_k)|} \end{bmatrix}^T \quad \text{and} \quad \mathbf{v}_2 = \frac{1}{\sqrt{2}} \begin{bmatrix} 1 \\ -\frac{\varphi(\tau_k)^*}{|\varphi(\tau_k)|} \end{bmatrix}^T.$$

Since λ_1 and λ_2 are also the two non-zero eigen-values of $\mathbf{C}(\tau_k) \mathbf{C}^H(\tau_k)$, the singular value decomposition (SVD) of the matrix $\mathbf{C}(\tau_k)$ is obtained as follows:

$$\mathbf{C}(\tau_k) = \mathbf{U}(\tau_k) \mathbf{\Sigma}(\tau_k)^{1/2} \mathbf{V}(\tau_k)^H, \quad (27)$$

where:

$$\mathbf{\Sigma}(\tau_k) \triangleq \text{diag}\{\lambda_1, \lambda_2\} \quad \text{and} \quad \mathbf{V}(\tau_k) \triangleq [\mathbf{v}_1 \ \mathbf{v}_2]. \quad (28)$$

Moreover, since $\mathbf{V}(\tau_k)^H \mathbf{V}(\tau_k) = \mathbf{I}_2$, then $\mathbf{U}(\tau_k) = [\mathbf{u}_1 \ \mathbf{u}_2]$ can be expressed as follows:

$$\mathbf{U}(\tau_k) = \mathbf{C}(\tau_k) \mathbf{V}(\tau_k)^H \mathbf{\Sigma}(\tau_k)^{-1/2}. \quad (29)$$

Therefore, it follows that:

$$\mathbf{u}_1 = \frac{1}{\sqrt{2\lambda_1}} \left(\mathbf{c}_1(\tau_k) + \frac{\varphi(\tau_k)^*}{|\varphi(\tau_k)|} \right), \quad (30)$$

$$\mathbf{u}_2 = \frac{1}{\sqrt{2\lambda_2}} \left(\mathbf{c}_2(\tau_k) - \frac{\varphi(\tau_k)^*}{|\varphi(\tau_k)|} \right). \quad (31)$$

Now, by injecting (27) back into (21), it follows that:

$$\mathbf{R}_{\mathbf{x}_k \mathbf{x}_k} = \sigma_{n_k}^2 \left(\frac{\rho_k}{2} \mathbf{B}(\nu_k, \tau_k) \mathbf{\Sigma}(\tau_k) \mathbf{B}(\nu_k, \tau_k)^H + \mathbf{I}_{Q_L} \right), \quad (32)$$

where $\mathbf{B}(\nu_k, \tau_k) = \mathbf{\Lambda}(\nu_k) \mathbf{U}(\tau_k)$ and $\rho_k = \sigma_{h_k}^2 / \sigma_{n_k}^2$ is the signal-to-noise ratio (SNR). Using the Woodbury identity [20] and exploiting the fact that \mathbf{u}_1 and \mathbf{u}_2 are orthogonal with unit norms, the inverse of the covariance matrix in (32) can be written as follows:

$$\mathbf{R}_{\mathbf{x}_k \mathbf{x}_k}^{-1} = \frac{1}{\sigma_{n_k}^2} \mathbf{I}_{Q_L} - \frac{1}{\sigma_{n_k}^2} \mathbf{B}(\nu_k, \tau_k) \mathbf{\Gamma}(\tau_k) \mathbf{B}(\nu_k, \tau_k)^H, \quad (33)$$

where:

$$\mathbf{\Gamma}(\tau_k) = \text{diag} \left\{ \frac{\rho_k \lambda_1}{2 + \rho_k \lambda_1}, \frac{\rho_k \lambda_2}{2 + \rho_k \lambda_2} \right\}. \quad (34)$$

And from (32), the determinant of $\mathbf{R}_{\mathbf{x}_k \mathbf{x}_k}$ can be obtained as:

$$\det\{\mathbf{R}_{\mathbf{x}_k \mathbf{x}_k}\} = \frac{(\sigma_{n_k}^2)^{Q_L}}{4} (\rho_k \lambda_1 + 2)(\rho_k \lambda_2 + 2). \quad (35)$$

By injecting (33) and (35) in (17), the LLF reduces to:

$$\mathcal{L}(\nu_k, \tau_k, \sigma_{n_k}^2) = -\ln((\rho_k \lambda_1 + 2)(\rho_k \lambda_2 + 2)) + \frac{1}{\sigma_{n_k}^2} \times \sum_{i=1}^2 \frac{\rho_k \lambda_i}{2 + \rho_k \lambda_i} \left| \sum_{m=0}^{Q_L-1} \mathbf{u}_i^*[m+1] e^{-j2\pi\nu\frac{m}{Q}} \mathbf{x}_k[m+1] \right|^2, \quad (36)$$

The LLF in (36) depends on both the target TD and CFO, but also on the Doppler spread. To reduce the complexity of the tri-dimensional estimation problem, we adopt an approach similar to the one in [8] to find the minimum of some cost function. This approach separates Doppler estimation from joint synchronization. We also use the TCC technique of Subsection III-A to obtain initial TD and CFO estimates, i.e., $\hat{\tau}_k^{(0)}$ and $\hat{\nu}_k^{(0)}$. The latter are then injected in the LLF of (36) to obtain an initial Doppler estimate. This preliminary guess is in its turn injected in the very same LLF function to jointly estimate the TD and CFO. The TCC-based technique is suitable for initialization since it provides good initial estimates for the TVC-based technique. Hence, the latter converges quickly, in few iterations only. The overall estimation technique at each relay R_k is summarized in Algorithm 1. Note also that the

Algorithm 1 Joint estimator for the Doppler, TD, and CFO at each relay R_K

Initialization: Estimate $\hat{\tau}_k^{(0)}$ and $\hat{\nu}_k^{(0)}$ using (15)
for $j = 1$ to J **do**
 Estimate $\hat{\sigma}_{D_k}^{(j)}$
 Estimate $\hat{\tau}_k^{(j)}$ and $\hat{\nu}_k^{(j)}$ using (36)
end for

estimates of the SNR, ρ_k , and the noise variance, $\sigma_{n_k}^2$, are obtained using the same approach adopted in [18].

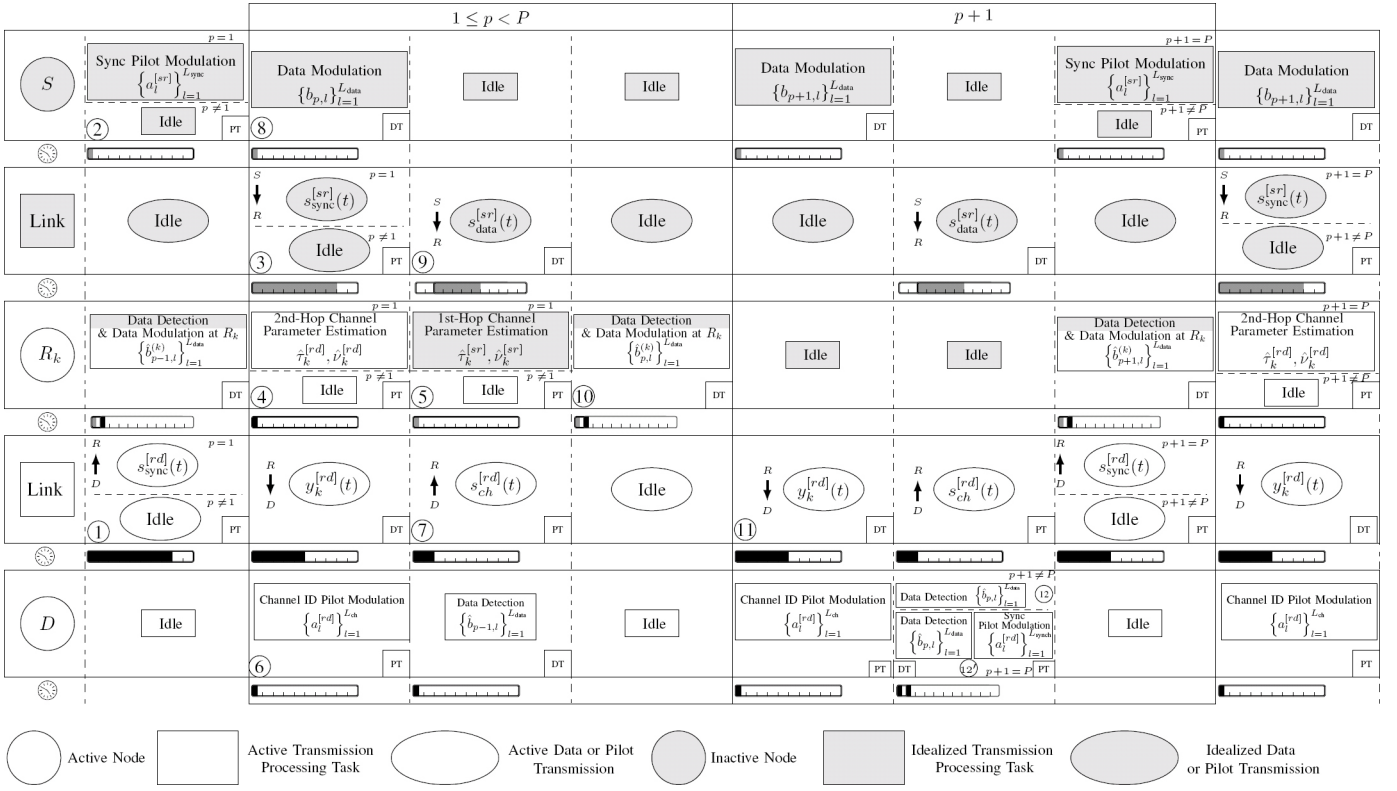


Fig. 2. Processing and data signaling structure of the two-hop MIMO-relay beamforming scheme assuming ideal (inactive) first-hop communication.

IV. DISTRIBUTED MIMO-RELAY BEAMFORMING

Very often, synchronization is performed at the destination where the receiver estimates all parameters. Many techniques opt for sub-optimal iterative implementations [8, 21] that could become ineffective in the case of dense networks. In such a case, open-loop synchronization architectures should be adopted instead. Accordingly, the proposed synchronization technique is run at each relay node. During a PT period, each node estimates the channel parameters. During the DT period, each relay will transmit the useful data to the destination while ensuring that the signal is modified properly using the TD, CFO, and channel estimates made available during the PT period. Full details of the processing and data signaling structure are shown in Fig. 2. Since the synchronization parameters are expected to vary with time, but actually at a rate much slower than the channel, the synchronization parameters are refreshed as shown in Fig. 2 once each P consecutive DT periods.

For more details about the proposed communication protocol, we provide an example on how the processing time and data signaling are organized in the time domain. In fact, during the first period, i.e., step (1), the destination broadcasts a training sequence, $\{a_l^{[rd]}\}_{l=1}^{L_{\text{sync}}}$, to all K relaying nodes. Then, the source node starts transmitting its own training sequence, $\{a_l^{[sr]}\}_{l=1}^{L_{\text{sync}}}$, to the relaying nodes during steps (2) and (3). Each relay node estimates the channel parameters $(\hat{\tau}_k^{[rd]}, \hat{\nu}_k^{[rd]})$

and $(\hat{\tau}_k^{[sr]}, \hat{\nu}_k^{[sr]})$ during steps (4) and (5), respectively. At steps (6) and (7), the destination node broadcasts another training sequence, $\{a_l^{[rd]}\}_{l=1}^{L_{\text{ch}}}$, dedicated to channel estimation. At the same time, the source node performs the same procedure by sending the sequence $\{b_{p,l}\}_{l=1}^{L_{\text{data}}}$ during steps (8) and (9). At step (10), each relay node uses $\hat{\tau}_k^{[sr]}$ and $\hat{\nu}_k^{[sr]}$ along with $\hat{h}_{k,p}^{[sr]}$ to estimate $\{\hat{b}_{p,l}^{(k)}\}_{l=1}^{L_{\text{data}}}$. The latter will be used along with $\hat{\tau}_k^{[rd]}, \hat{\nu}_k^{[rd]}$, and $\hat{h}_{k,p}^{[rd]}$ to generate the transmitted signal $y_k^{[rd]}(t)$. The signal $y_k^{[rd]}(t)$ is transmitted during step (11). Finally, the destination node performs a simple decoding procedure during step (12). During the next $P - 1$ periods (i.e., $1 < p < P$), steps (1) to (5) are ignored since the channel parameters $(\hat{\tau}_k^{[rd]}, \hat{\nu}_k^{[rd]})$ and $(\hat{\tau}_k^{[sr]}, \hat{\nu}_k^{[sr]})$ are assumed to be the same over P periods. At the P^{th} period, however, we execute the same steps (6) to (11) but slightly change the final step (12) and, hence, denote it as (12'). In step (12'), once the destination node completes the decoding process, it starts broadcasting again the very same training sequence $\{a_l^{[rd]}\}_{l=1}^{L_{\text{sync}}}$.

V. SIMULATION RESULTS

In the following, we discuss our simulation results at both the component and link levels when all previous works would stop short from moving to the more time consuming yet much more insightful link-level throughput metric. In all our simulations, we assume as would be expected in practice that the K relays are co-located at about the same distance and moving at

the same relative speed from the destination whether the latter is stationary or also in motion itself. Under this assumption, the average SNR and the Doppler frequency are assumed to be the same over all R-D and D-R links. In the following, we will investigate in different scenarios the estimation accuracy of the tested synchronization parameter estimators in terms of the normalized mean square error (NMSE) before assessing their link-level throughput performance.

A. Component-Level Simulations

In all component-level simulations, we consider a training sequence, $\mathbf{a}^{[dr]}$, of $L_{\text{sync}} = 128$ QPSK symbols and a square root raised-cosine shaping-pulse filter (SRRC) with a roll-off factor $\rho = 0.3$. In Fig. 3, we compare the proposed technique under its two variants with idealized and active Doppler frequency estimation, i.e., ML TVC-PD (perfect Doppler) and ML TVC-DE, against the space alternating generalized expectation maximization (SAGE) algorithm in [8], the sole benchmark available in the literature dealing with multi-node TD and CFO synchronization, and the CRLBs in terms of NMSE performance. We observe that all tested techniques

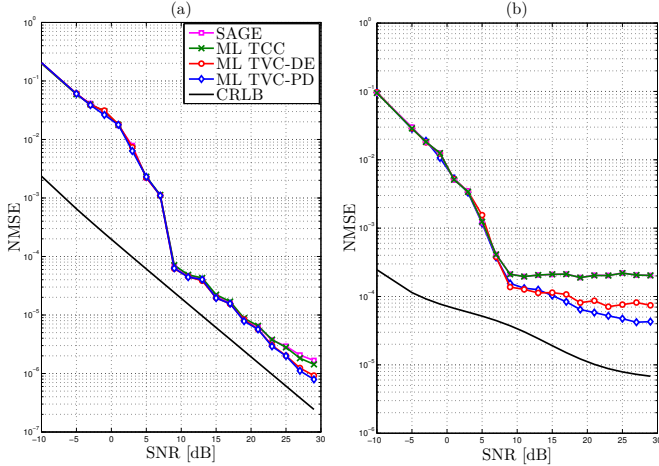


Fig. 3. CRLB and NMSE vs SNR of the ML TVC, ML TCC, and SAGE techniques vs the SNR with $F_{D_k} = 15$ Hz and *uniform Jakes'* model for: (a) the TDs and (b) the CFOs.

perform nearly the same at $F_{D_k} = 15$ Hz with a small advantage for both TVC-PD and TVC-DE at high SNR. On the other hand, SAGE and ML TCC - which perform exactly the same because they both rely on the TCC assumption - see their performance slightly degrade at high SNR because the channel is not totally constant (i.e., $F_{D_k} \neq 0$ Hz). Besides, we observe that ML TVC-DE matches its idealized ML TVC-PD counterpart in terms of TD estimation accuracy whereas it exhibits slightly lower CFO estimation performance. In fact, this degradation stems from the Doppler estimation errors that increase at higher Doppler with more detrimental impact on CFO estimation.

In Fig. 4, we tackle the more challenging case of a much significantly higher Doppler $F_{D_k} = 100$ Hz. Here again, we can report the very same qualitative observations of Fig. 3, yet with more prominent performance gaps this time in terms

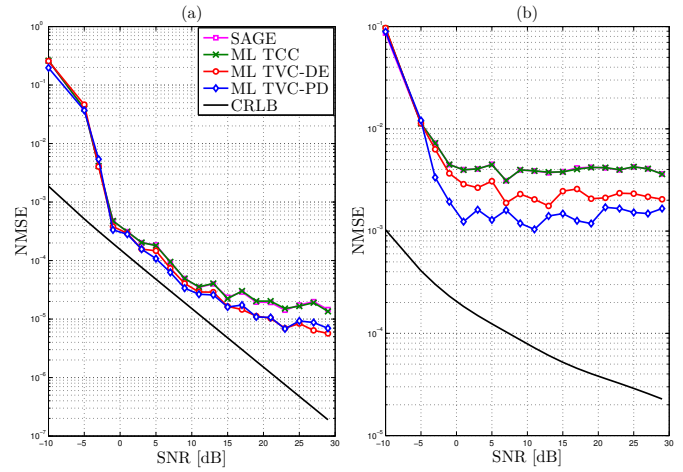


Fig. 4. CRLB and NMSE vs SNR of the ML TVC, ML TCC, and SAGE techniques vs the SNR with $F_{D_k} = 100$ Hz and *uniform Jakes'* model for: (a) the TDs and (b) the CFOs.

of CFO and TD estimation accuracies, more so at high SNR, between on one hand ML TVC and the TCC-based techniques (i.e., SAGE and ML TCC) and on the other hand between ML TVC-PD and ML TVC-DE. This is hardly surprising because on one hand SAGE and ML TCC fail to reach the global maximum and exhibit poor performance since the TCC assumption no longer holds at high Doppler. And because, on the other hand, the Doppler estimator selected for joint operation with the new ML TVC technique to illustrate its applicability in real-world operating conditions is specifically tailored to cope with the far more challenging estimation of low Doppler frequencies. As such, the additional performance losses resulting from the joint estimation of high Doppler can be reduced to the same negligible gaps observed in Fig. 3 at low Doppler; that is by the simple integration of alternative Doppler estimators more easily tailored to be more accurate at high Doppler.

B. Link-Level Simulations

Our link-level simulations were run using the key setup parameters listed in Table I.

TABLE I
SIMULATION PARAMETERS

Parameters	Symbol	Values
Symbol period	T	1/14 ms
Number of relays	K	{1, 2, 4, 8}
Maximum Doppler shift	$\{F_{D_k}\}_{k=1}^K$	{15, 100, 200, 300} Hz
Oversampling factor	Q	2
Roll-off factor	ρ	0.3
TDs	τ_k	Uniformly random (i.i.d.)
CFOs	ν_k	Uniformly random (i.i.d.)
$R_k - D$ channel	\mathbf{h}_k	Rayleigh random (i.i.d.)

Fig. 5 depicts the resulting throughput for three different modulation orders (QPSK, 16-QAM and 64-QAM) and K relays. We consider in Figs. 5 (a) and 5 (b) the case where all K relay-destination links have the same maximum Doppler frequency shift of 15 and 100 Hz, respectively. For a given

modulation order M , the throughput is obtained from the symbol error rate (SER) as follows:

$$\text{Throughput} = \frac{1}{T} \log_2(M)(1 - \text{SER})(1 - R), \quad (37)$$

where R is the overhead ratio. Note here that the latter is computed over a period that spans L_{sync} symbols for synchronization and P periods each of which includes $L_{\text{ch}} = 2$ pilot symbols followed by $L_{\text{data}} = 12$ information-bearing symbols. As such, the overhead ratio is given by:

$$R = \frac{L_{\text{sync}} + L_{\text{ch}}P}{L_{\text{sync}} + (L_{\text{ch}} + L_{\text{data}})P}. \quad (38)$$

Our simulations were obtained for $L_{\text{sync}} = 128$ and $P = 100$. Note here that the overhead ratio associated with the synchronization period becomes negligible for such large value of P . The latter cannot, however, be increased indefinitely as it is dictated by the required refreshment rate P that better copes with the time variations of the synchronization parameters.

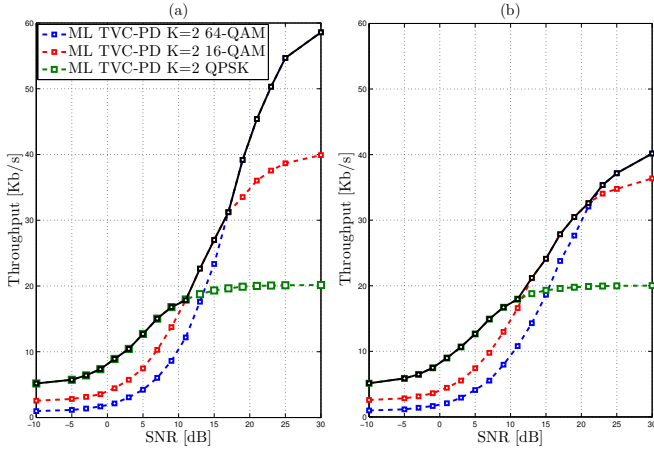


Fig. 5. Link-level throughput vs SNR for ML TVC-PD at $K = 2$ relays and a refreshment rate $P = 100$ for: (a) $\{F_{D_k}\}_{k=1}^K = 15$ Hz, and (b) $\{F_{D_k}\}_{k=1}^K = 100$ Hz.

We see from Fig. 5 (a) that QPSK transmissions, among the different considered modulations, provide higher throughput for SNR values below 11 dB. When the SNR ranges between 11 dB and 16 dB, 16-QAM becomes more suitable whereas 64-QAM dominates when the SNR exceeds 16 dB. The resulting throughput curve assuming an adaptive (i.e., SNR-dependent) modulation is depicted by the black curve.

In Fig. 5 (b), we show the performance of the proposed distributed beamforming scheme at a higher Doppler $F_{D_k} = 100$ Hz (i.e., fast TVCs). In this scenario, QPSK and 16-QAM provide higher throughput over the same SNR ranges reported above at low Doppler whereas 64-QAM dominates when the SNR exceeds 21 dB. We also observe that 64-QAM transmissions suffer from a noticeable performance degradation. Indeed, at lower Doppler, the phase estimates provide accurate values since the channel varies slowly during the same period. Hence, the decoder at the destination is able to accurately estimate the transmitted symbols. In the case of high mobility, the channel varies rapidly during the same

period, leading to a more severe degradation of the channel estimates. The latter affects the decoding process, especially at higher modulations which are more sensitive to phase shifts.

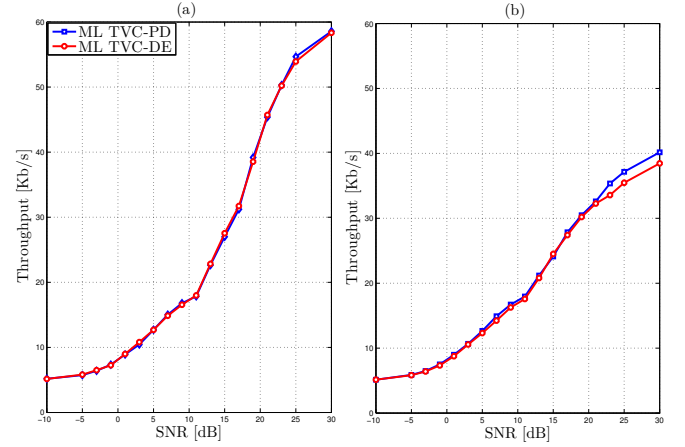


Fig. 6. Link-level throughput vs SNR for ML TVC-PD and ML TVC-DE at $K = 2$ relays, $\{F_{D_k}\}_{k=1}^K = 100$ Hz, and a refreshment rate $P = 100$ for: (a) $\{F_{D_k}\}_{k=1}^K = 15$ Hz, and (b) $\{F_{D_k}\}_{k=1}^K = 100$ Hz.

In Fig. 6, we compare ML TVC-DE and ML TVC-PD in terms of throughput. The former sees its performance deteriorate against the latter only at high SNR. Losses are negligible at low Doppler, but become noticeable at high Doppler. Yet, as reported previously when discussing the component-level simulation results, such link-level throughput gap can be easily bridged by the integration of an alternative high-range Doppler estimator, thereby making ML TVC-PD equivalent to ML TVC-DE and a meaningful version in what follows for further comparisons with existing Doppler-independent TCC-based benchmarks.

In Fig. 7, we compare the performance of ML TVC-PD, ML TCC, and SAGE in terms of throughput for different numbers of relays (i.e., $K = 1, 2, 4$, and 8) and four different Doppler frequencies (i.e., $\{F_{D_k}\}_{k=1}^K = 15$ Hz, 100 Hz, 200 Hz, and 300 Hz). We see under the TCC assumption (i.e., $F_{D_k} = 15$ Hz) that all techniques perform nearly the same in terms of link-level throughput. They do so the best with QPSK when the SNR is below 11 dB whereas 16-QAM becomes more suitable at SNR values ranging from 11 to 16 dB. When the SNR exceeds 16 dB, 64-QAM ultimately becomes the best choice. At higher Doppler (i.e., $F_{D_k} = 100$ Hz), we can always report noticeable and constantly increasing throughput gains of ML TVC over TCC-based SAGE and ML TCC at both medium and high SNR when increasing the number of relays from 1 to 8. At lower SNR, all techniques exhibit the same NMSE and consequently the same throughput. At even higher Doppler (i.e., $F_{D_k} = 200, 300$ Hz), the relative throughput gains of ML TVC over SAGE and ML TCC become even more significant, again more so when the number of relays also increases. These key observations come as a solid confirmation of the key performance benefits of the proposed distributed MIMO-relay beamforming and multi-node synchronization schemes.

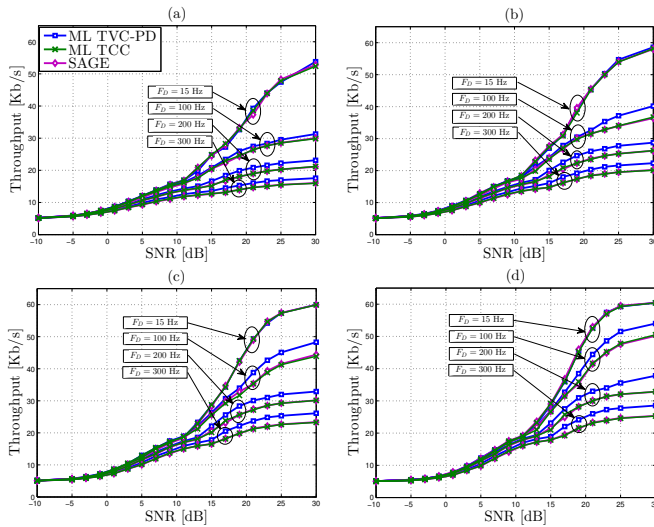


Fig. 7. Link-level throughput vs SNR for ML TVC-PD at a refreshment rate $P = 100$ and different Doppler frequencies for: (a) $K = 1$, (b) $K = 2$, (c) $K = 4$, and (d) $K = 8$.

VI. CONCLUSION

In this paper, we addressed the problem of time and frequency synchronization in cooperative systems over TVCs. We proposed two different estimation techniques. The first operates under the TVC assumption while the second one works with TCCs. In the first ML TVC-DE approach, we exploit the second ML TCC technique as an initialization scheme for preliminary synchronization. We also developed a new distributed MIMO-relay beamforming design that embeds the proposed synchronization technique at each relay node. We showed under the TCC assumption that all techniques exhibit approximately the same performance. However, when the Doppler increases, the TCC-based techniques exhibit poor performance while the new ML TVC continues to provide accurate estimates. Link-level simulations confirm the net advantages of the proposed ML TVC multi-node synchronization technique and the MIMO-relay beamforming scheme in terms of throughput gains, especially at medium and high SNRs, more so at relatively higher Doppler frequencies or with more distributed MIMO-relay beamforming nodes.

REFERENCES

- [1] S. Ben Amor, S. Affes, F. Bellili, U. Vilaipornsawai, L. Zhang, and P. Zhu, "Multi-node ML time and frequency synchronization for distributed MIMO-relay beamforming over time-varying flat-fading channels," *IEEE Trans. on Commun.*, appeared online, Dec. 2018, DOI: 10.1109/TCOMM.2018.2889089.
- [2] Y. Jing and H. Jafarkhani, "Network beamforming using relays with perfect channel information," *IEEE Trans. Inf. Theory*, vol. 55, no. 6, pp. 2499-25178, June 2009.
- [3] A. A. Nasir, S. Durrani, H. Mehrpouyan, S. D. Blostein, and R. A. Kennedy, "Timing and carrier synchronization in wireless communication systems: a survey and classification of research in the last 5 years," *EURASIP J. Wirel. Commun. Netw.*, vol. 58, no. 4, pp. 1-38, Dec. 2016.
- [4] X. Li, C. Xing, Y.-C. Wu, and S. C. Chan, "Timing estimation and resynchronization for amplify-and-forward communication systems," *IEEE Trans. Signal Process.*, vol. 58, no. 4, pp. 2218-2229, Apr. 2010.
- [5] X. Li, Y. C. Wu, and E. Serpedin, "Timing synchronization in decode-and-forward cooperative communication systems," *IEEE Trans. Signal Process.*, vol. 57, no. 4, pp. 1444-1455, Apr. 2009.
- [6] H. Mehrpouyan and S. D. Blostein, "Bounds and algorithms for multiple frequency offset estimation in cooperative networks," *IEEE Trans. Wireless Commun.*, vol. 10, no. 4, pp. 1300-1311, Apr. 2011.
- [7] T. Pham, A. Nallanathan, and Y. Liang, "Joint channel and frequency offset estimation in distributed MIMO flat-fading channels," *IEEE Trans. Wireless Commun.*, vol. 7, no. 2, pp. 648-656, Feb. 2008.
- [8] A. A. Nasir, H. Mehrpouyan, S. Durrani, R. A. Kennedy, and S. D. Blostein, "Timing and carrier synchronization with channel estimation in multi-relay cooperative networks," *IEEE Trans. Signal Process.*, vol. 60, no. 2, pp. 793-811, Feb. 2012.
- [9] S. Chakraborty and D. Sen, "Joint estimation of time, frequency offsets, and channel gains with ICIs in EF multi-relay DMIMO-OFDM system," *IEEE Trans. on Veh. Technol.*, vol. 66, no. 7, pp. 5822-5838, Jul. 2017.
- [10] S. Jayaprakasam, S.K. Abdul Rahim, and C.Y. Leow, "Distributed and collaborative beamforming in wireless sensor networks: classifications, trends, and research directions," *IEEE Commun. Surv. Tut.*, vol. 19, no. 4, pp. 2092-2116, Q4, 2017.
- [11] H. Yang, D. Liu, Y. Fan, C. Qian, Z. Zheng, and B. Yan, "Variable directional perturbation with one-bit feedback for collaborative beamforming," in *Proc. IEEE/CIC ICC*, 2016.
- [12] F. Quitin, M. M. Ur Rahman, R. Mudumbai, and U. Madhoo, "Distributed beamforming with software-defined radios: Frequency synchronization and digital feedback," in *Proc. IEEE GLOBECOM*, 2012, pp. 4787-4792.
- [13] M.A. Alvarez and U. Spagnolini, "Distributed time and carrier frequency synchronization for dense wireless networks," *IEEE Trans. Signal Inform. Process. Netw.*, pp. 1-13, Mar. 2018.
- [14] R. He, G. Wang, Z. Zhong, A.F. Molisch, C. Briso-Rodriguez and C. Oestges, "High-speed railway communications: From GSM-R to LTE-R," *IEEE Trans. Veh. Technol. Mag.*, vol. 11, no. 3, pp. 49-58, Mar. 2016.
- [15] I. Thibault, G.E. Corazza, and L. Deambrogio, "Phase synchronization algorithms for distributed beamforming with time varying channels in wireless sensor networks," in *Proc. IEEE IWCMC*, 2011, pp. 77-82.
- [16] W. Tushar, D.B. Smith, A. Zhang, T.A. Lamahewa, and T. Abhayapala, "Distributed transmit beamforming: Phase convergence improvement using enhanced one-bit feedback," in *Proc. IEEE WCNC*, 2012, pp. 528-532.
- [17] S. Ben Amor, S. Affes, F. Bellili, U. Vilaipornsawai, L. Zhang, and P. Zhu, "ML time-delay and CFO synchronization for MIMO-relay beamforming over time-varying channels," in *Proc. IEEE GLOBECOM*, 2018, to appear.
- [18] M. Souden, S. Affes, J. Benesty, and R. Bahroun, "Robust Doppler spread estimation in the presence of a residual carrier frequency offset," *IEEE Trans. Signal Process.*, vol. 57, no. 10, pp. 4148-4153, Oct. 2009.
- [19] F. Bellili, Y. Selmi, S. Affes, and A. Ghayeb, "A low-cost and robust maximum likelihood joint estimator for the Doppler spread and CFO parameters over flat-fading Rayleigh channels," *IEEE Trans. Commun.*, vol. 65, no. 8, pp. 3467-3478, Aug. 2017.
- [20] K.B. Petersen and M.S. Pedersen, *The Matrix Cookbook*, Technical University of Denmark, Nov. 2012, Ref. 20121115.
- [21] Y. Tian, X. Lei, Y. Xiao, S. Li, "SAGE based joint timing-frequency offsets and channel estimation in distributed MIMO systems," *Elsevier J. Comput. Commun.*, vol. 33, no. 17, pp. 2125-2131, July 2010.